Point spread function of the optical needle super-oscillatory lens

Tapashree Roy,[1] Edward T. F. Rogers,[1,2] Guanghui Yuan,[3] and Nikolay I. Zheludev[1,3,a]

[1]*Optoelectronics Research Centre and Centre for Photonic Metamaterials, University of Southampton, Highfield, Southampton, SO17 1BJ, United Kingdom*
[2]*Institute for Life Sciences, University of Southampton, Highfield, Southampton, SO17 1BJ, United Kingdom*
[3]*Centre for Disruptive Photonic Technologies, Nanyang Technological University, Singapore 637371*

Super-oscillatory optical lenses are known to achieve sub-wavelength focusing. In this paper, we analyse the imaging capabilities of a super-oscillatory lens by studying its point spread function. We experimentally demonstrate that a super-oscillatory lens can generate a point spread function 24% smaller than that dictated by the diffraction limit and has an effective numerical aperture of 1.31 in air. The object-image linear displacement property of these lenses is also investigated. © 2014 AIP Publishing LLC. [http://dx.doi.org/10.1063/1.4882246]

Diffraction causes the image of a point object to appear as a hotspot of finite radius accompanied by annular bands, even when observed through an ideal lens. The intensity distribution of the image of the point object is commonly known as the point spread function (PSF).[1] The specific form of this PSF for an ideal lens is known as the Airy pattern after the 19th century astronomer Sir George Biddell Airy who was the first to describe such spreading of light.[2] The minimum radius of the hotspot of an Airy pattern is limited by diffraction, with full width at half maximum (FWHM) measuring $\lambda/2\text{NA}$ (where λ is the wavelength and NA is the numerical aperture of the microscope objective). For normal incoherent imaging, the image of an extended object is the convolution of the object with the PSF of the system, and hence, the size of the PSF determines the resolution of the microscope. Methods of reducing the size of the PSF of an optical system by using modified pupil functions were first described in 1952 by Toraldo di Francia[3] and they have since been studied extensively (for a recent review see Ref. 4) and their use in practical imaging systems has also been demonstrated.[5–11]

Recently, a class of optical lenses based on the principle of super-oscillation[12,13] has been proven to focus light smaller than the diffraction limit. One method of creating sub-diffraction super-oscillatory optical hotspots is using suitably designed amplitude masks.[14,15] Such super-oscillatory lenses (SOLs) have been used in a scanning imaging system[16] to resolve a pair of 200 nm diameter holes with edge-to-edge separation of 105 nm with 640 nm light. Besides optimized amplitude masks, super-oscillatory hotspots may also be realized by using a spatial light modulator and a conventional optical microscope.[17–20] In these methods, optical eigenmodes may be used to determine the required amplitude and/or phase modulation to produce the smallest possible focal spot after the objective lens. Using this technique, super-resolution imaging was experimentally demonstrated in a low NA imaging system providing 1.3 times improvement over the diffraction limit.[19] The spatial light modulator can also be used in the collection path of a conventional microscope for super-oscillatory filtering of the captured images, thus increasing the resolution of the imaging system.[10,11]

The amplitude mask type SOLs are known to demonstrate sub-wavelength focal spots with effective NA higher than conventional lenses.[15] A variation of the SOL as presented in Ref. 16 focuses light into a sub-wavelength needle and is termed the optical needle super-oscillatory lens (ONSOL).[21] In our previous papers,[16,21] we have studied the plane wave focusing characteristics of the SOL and the ONSOL. In this paper, we study the imaging performance of a super-oscillatory microscope in which the imaging objective is replaced by either a SOL or an ONSOL. We study how accurately the SOL or the ONSOL can image a point object, i.e., their point spread functions are characterized. We demonstrate that a super-oscillatory lens reduces the size of the point spread function below the conventional diffraction limit. In the following sections, we present a numerical study comparing the PSF formed by a SOL and an ONSOL. It will be demonstrated that for a given object and image distance, the PSF formed by an ONSOL is more robust to any object displacement in the direction perpendicular to the optical axis. After establishing that the ONSOL is a better choice than the SOL for practical imaging and lithography applications, we will present an experimental study of the ONSOL imaging performance.

Figure 1 shows a simulated comparison between the PSFs formed by a SOL and an ONSOL. Our numerical investigations show[22] that both the SOL and the ONSOL form sub-wavelength PSFs at $9\,\mu\text{m}$ from the respective lenses when a point object is placed $25\,\mu\text{m}$ away on the other side of the lenses (Fig. 1(a)). It must be noted that both of these super-oscillatory lenses also form sub-wavelength PSFs at other object-image distance pairs, but these may not be the same for each of them. The above object-image distance is chosen so that direct comparison can be drawn between imaging performance of the two super-oscillatory lenses.

We simulate the propagation of light from the point object to the lenses and onto the image plane, using the scalar angular spectrum method,[23] which has previously been shown to be suitable for these types of propagation problems.[21] Monochromatic light with wavelength 640 nm from a luminous point object ($\sim$100 nm diameter) propagates through free space and illuminates each lens (positioned $25\,\mu\text{m}$ from the source, see Fig. 1(a)). To ensure that the
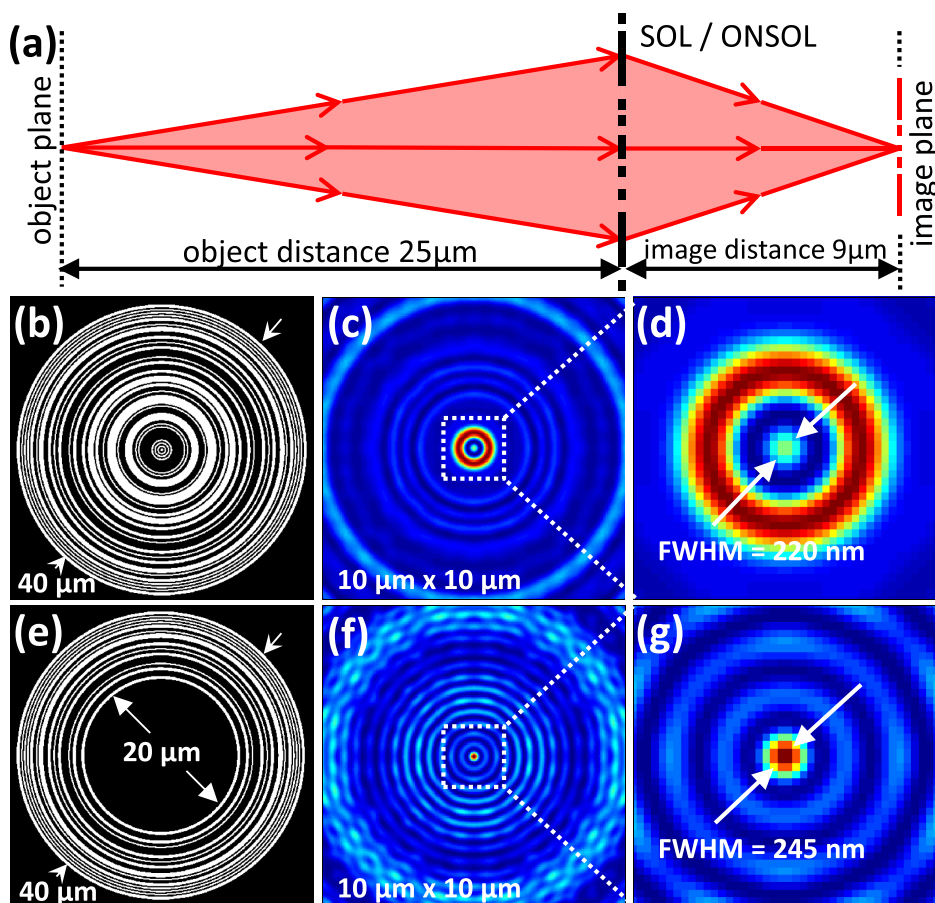
a)niz@orc.soton.ac.uk

FIG. 1. Super-oscillatory point spread functions. (a) Ray diagram showing image formation by super-oscillatory lenses. Mask designs of (b) SOL, and (e) ONSOL. PSF generated 9 μm away from (c) SOL and (f) ONSOL when a 100 nm circular aperture is placed 25 μm away. Central intensity distribution of PSF generated by (d) SOL and (g) ONSOL, $\lambda = 640$ nm. Intensities in (f) and (g) are 11 times stronger than that in (c) and (d).

chosen size of the aperture is small enough to be considered as a point source, simulations (not shown here) are done with different aperture sizes. For apertures smaller than 200 nm, the PSF does not vary with changing source size. An aperture diameter of 100 nm is chosen to match the experimentally used point source.

The designs of the super-oscillatory lenses are shown in Figs. 1(b) and 1(e), respectively. The designs are identical except that the center of the ONSOL is blocked by a 20 μm diameter disc. This blocking region helps the ONSOL push high intensity sidebands away from the central spot, while the remaining peripheral rings ensure that the high wave vectors required for producing sub-diffraction-limited focal spots are preserved.[21] The increased field of view makes the ONSOL a more practical choice over the SOL for applications such as photolithography. Figures 1(c) and 1(d) show the PSF generated by the SOL, with a hotspot measuring 0.35 λ and accompanied by an intense ring around the spot. The peak intensity of the central hotspot is 0.5 times that of the first annular ring. The ONSOL generates a PSF with a hotspot measuring 0.38 λ, still beating the diffraction limit but with much lower intensity annular rings (Figs. 1(f) and 1(g)). In the case of ONSOL, the central peak is 4.5 times that of the first annular ring. For comparison, a high NA (0.95) microscope objective would form a PSF with the hotspot FWHM measuring $\sim$0.53λ. For a conventional lens, the FWHM of the PSF is given by $\lambda/2\text{NA}$. We therefore define an effective NA for our super-oscillatory lenses as $\text{NA}_{\text{eff}} = \lambda/2\text{FWHM}_{\text{PSF}}$. Using this formula, we calculate $\text{NA}_{\text{eff, SOL}} = 1.43$ and $\text{NA}_{\text{eff, ONSOL}} = 1.31$; note that the maximum possible NA for any conventional lens in air is 1.

Next, we investigate another lens-like function of our super-oscillatory lenses. For any ordinary lens, if a point object is displaced perpendicular to the optical axis, the image moves linearly in the opposite direction. This is because a shift in the position of the object causes a wavefront tilt at the lens plane and hence a shift in position of the image spot. We expect the same principle should apply to super-oscillatory lenses. As we will see below, this lens-like function of the super-oscillatory lenses holds true only for small object displacements because of the complicated transmission function of the lens. We have also found that this lens-like object-image displacement holds true for several object-image distance pairs (see supplementary material[22] for experimental study).

In the simulations, we displace a point object perpendicular to the optical axis of the super-oscillatory lenses and watch the corresponding image displacement. The object-image distances are kept the same as the last simulation (Fig. 1(a)) for both the SOL and the ONSOL. Figures 2(d)–2(g) show the image displacement for SOL when the luminous point object is displaced by 3 μm perpendicular to the optical axis. When the point source is perfectly aligned with the optical axis (Fig. 2(d)), the PSF appears same as in Fig. 1(b); note the difference in appearance is only due to different colour scales for intensities. As the point object is displaced from the optical axis the image moves opposite to the direction of object movement, as would happen for an ordinary lens. The central spot in the PSF moves by 500 nm for every 1 μm object movement. At the same time, the central spot distorts and decreases sharply in intensity while the

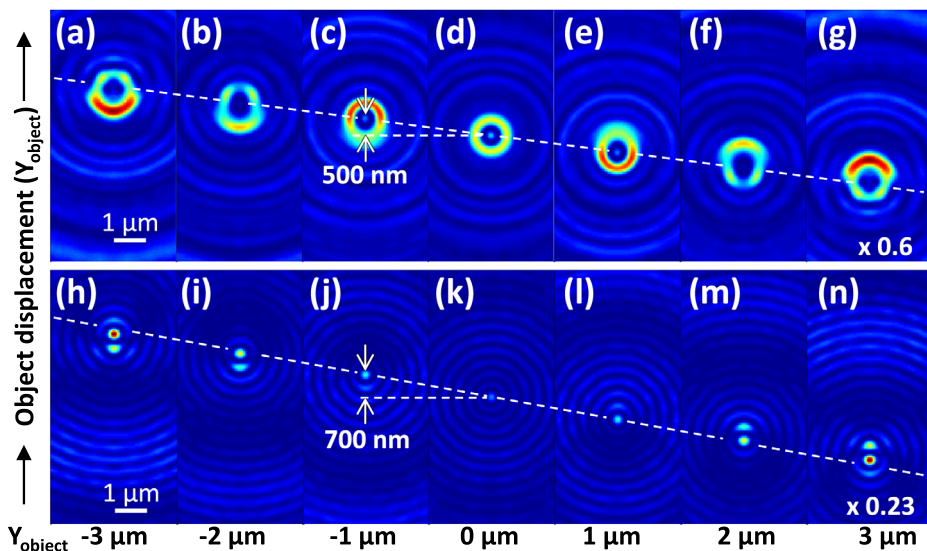FIG. 2. Object-image displacement: SOL vs. ONSOL. A point object is displaced laterally by 3 μm on either side of the optical axis of the lenses. Corresponding displacement of the PSF formed by SOL (a)–(g) and ONSOL (h)–(n). Colour scale for intensities in (a)–(g) is 0.6 times of that in Fig. 1(c) and that in (h)–(n) is 0.23 times of that in Fig. 1(f).

sidebands increase in intensity and become more and more asymmetric. When the object is displaced by 3 μm, the central spot becomes difficult to recognize (Fig. 2(g)). The trend is the same as the point object moves to the other side of the optical axis (Figs. 2(d)–2(a)). For the ONSOL, the direction of relative movement of the point source and the PSF is the same as in the case of the SOL. Interestingly, the ONSOL PSF is more robust to object displacement than that of the SOL. This is primarily due to the difference in intensity of the closest sidebands for the two lenses. For the SOL, even a small distortion of the highly intense sidebands is sufficient to mask the central hotspot. For the ONSOL, on the other hand, the sidebands immediately surrounding the central hotspot are weaker than the spot itself, and hence larger distortions (and larger object displacements) are tolerable. The intensity content in the central spot of the ONSOL increases with displacement of the point source (Figs. 2(k)–2(n)). The central spot is still recognizable when the object is displaced 3 μm off the axis, though the spot becomes slightly elliptical. As with the SOL, the sidebands for the ONSOL become more and more asymmetric with increasing off-axis object placement, though most of the energy remains in the central spot. For both the super-oscillatory lenses, this distortion of the image with off-axis object placement happens because the super-oscillatory PSFs are formed by delicate interference of a large number of beams, and any misalignment of the point source is transferred to the image plane as distortion of the sidebands and the central spot.

Note that for the ONSOL, the central spot in the PSF moves by 700 nm for every 1 μm object movement (Figs. 2(j) and 2(k)). This is different to that of the SOL, even though the object and image positions remain the same. As the SOL and the ONSOL both display complex (and significantly different) focusing behaviour, it is reasonable that their imaging characteristics are slightly different even for the same pair of object and image distances. Also note that compared to the SOL, the ONSOL is characterized by an increased field of view and robustness of the super-oscillatory sub-wavelength PSF to off-axis placement of the object. These features make the ONSOL a promising choice for high speed processing applications including imaging

and photolithography. Therefore, we will test the experimental performance of imaging with ONSOL.

Figure 3 shows an experimental demonstration of point-object imaging capabilities of an optical needle super-oscillatory lens. The lens (Fig. 3(a)) is fabricated by focused ion beam milling of a 100 nm thick gold layer deposited on a 50 nm thick silicon nitride membrane. To approximate the point source, a 640 nm linearly polarized laser is coupled into a scanning near field optical microscope (SNOM) probe with 100 nm aperture at the tip. A conventional microscope with high NA objective (Nikon CFI LU Plan Apo EPI 150X, NA = 0.95) is used to record the PSF created by the ONSOL. Since the super-oscillatory PSFs are formed by interference of propagating waves, they can be imaged by a conventional objective. The imaging objective is kept fixed at 9 μm from the ONSOL—as in the simulations. The SNOM tip is placed on the optical axis and moved away from the ONSOL in 100 nm steps, to find the object position that forms a PSF with sub-diffraction-limited central hotspot at the fixed 9 μm
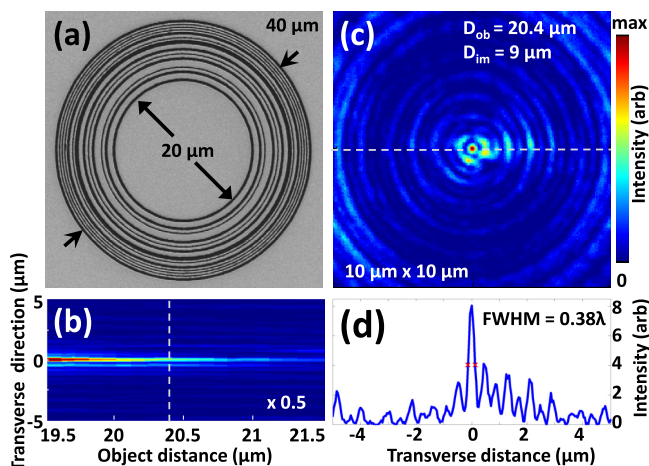

FIG. 3. ONSOL generated PSF: experimental result. (a) SEM image of the ONSOL. (b) Axial intensity distribution of the PSF over the distance where the hotspot is smaller than the diffraction limit. (c) Intensity distribution of the PSF for object distance = 20.4 μm and image distance = 9 μm, colour scale for intensity is 2 times that of (b). (d) Intensity profile through the line in (b) and (c).
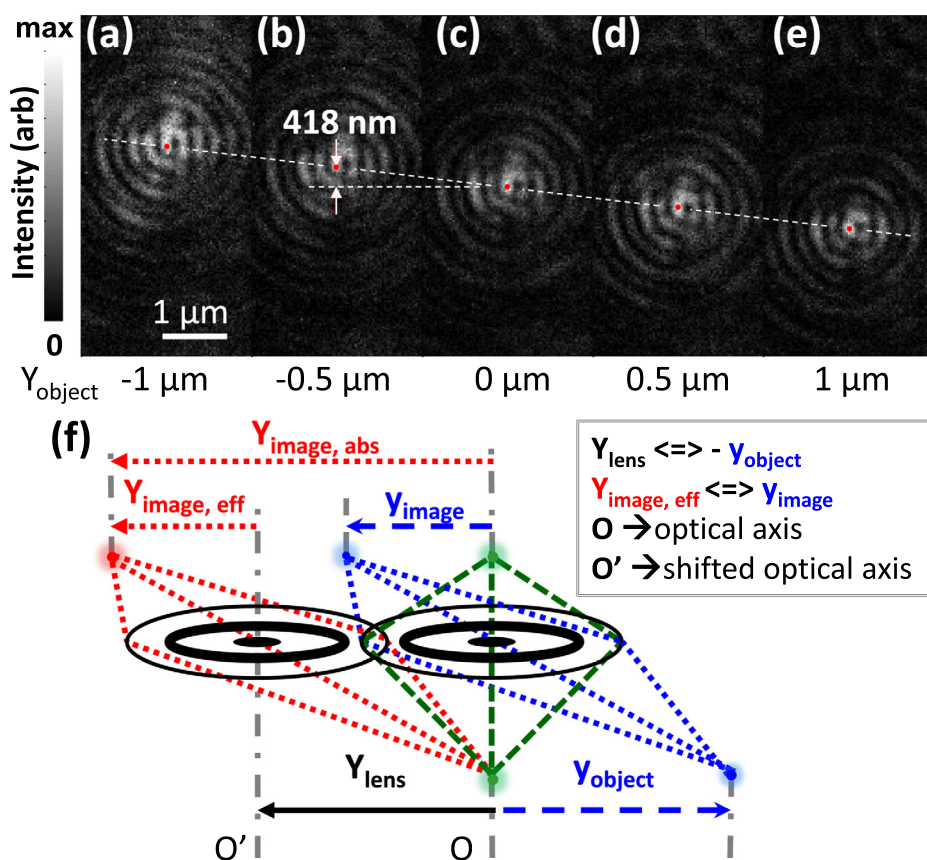
FIG. 4. ONSOL vs. image displacement: experimental result. The ONSOL is displaced by 500 nm between each frame showing total $2\,\mu$m displacement between (a) and (e). (Multimedia view) [URL: http://dx.doi.org/10.1063/1.4882246.1]. (f) Schematic showing the equivalence between object displacement (in blue) and lens displacement (in red); the original undisturbed position for object, lens, and image is shown in green.

imaging distance. Experimentally, we find this PSF when the tip is 19.5 μm from the ONSOL and the PSF remains sub-diffraction-limited for the next $2\,\mu$m along the propagation direction (Fig. 3(b)). In fact, our simulation results show that with the imaging plane fixed at 9 μm, the PSF formed by this ONSOL remain continuously sub-diffraction-limited for object distances between 11.5 μm and 30 μm.[22] In our experiment, sub-wavelength PSF is found over a shorter object-distance probably due to mechanical drifts in the real imaging system. However, this extended focal depth of the ONSOL means it is not ideal for imaging of 3D objects, but is useful for imaging planar surface, since it allows a large tolerance in the placement of the object. As an example of the sub-diffraction PSF in the transverse plane, the intensity distribution along the dashed line in Fig. 3(b) is plotted in Fig. 3(c), when the point source is 20.4 μm from the lens. As in the computational results, the hotspot in the PSF has FWHM = 0.38λ (Fig. 3(d)) surrounded by low intensity sidebands. The slight asymmetry in the PSF is probably due to a small displacement of the point source from the optical axis of the lens; the same effect as seen in the simulations above.

To experimentally verify the correlation between object and image displacement for the optical needle lens, the lens is placed on a piezo-stage (P-545, Physik Instrumente) and moved in 100 nm steps over a distance of $4\,\mu$m perpendicular to the optical axis. For each position, the image displacement is recorded by the microscope and CCD camera. Figures 4(a)–4(e) present the experimental image shift when the ONSOL moves by 1 μm on either side of central position. Each image is re-positioned so that the optical axis of the ONSOL is held at zero displacement to facilitate comparison

with the simulations (Fig. 4(f)). A video with the full set of experimental data as acquired is available online (Figs. 4(a)–4(e), multimedia view). In this experiment, the point source is 17.6 μm from the ONSOL, and imaged at 9 μm. This object-image distance pair has shown the best experimental demonstration of image displacement. However, image displacement for other object-image distance pairs, including those where the PSF is considerably sub-diffraction-limited, have been experimentally studied.[22] In the case of Figs. 4(a)–4(e), the hotspots measure 0.48λ, which is still smaller than the diffraction-limit. It is found in the experiment that for every 500 nm displacement of the object, the image moves by 418 nm in the other direction. This is very close to the simulations done for this particular object-image distance pair, where the corresponding image shift is 415 nm.

In conclusion, we have demonstrated that the point spread functions generated by super-oscillatory binary lenses have hotspot radii 24% smaller than the diffraction-limited lenses and the effective numerical aperture in air is 1.31, demonstrating their usefulness for super-resolution imaging applications. Of the two types of super-oscillatory lenses investigated, the optical-needle type creates a PSF with less intense sidebands and is more robust to off-axis object placement than a standard SOL. This makes the ONSOL a promising choice for super-resolution microscopy of planar objects and photolithography. Area imaging with super-oscillatory lenses has significant speed advantages over previously demonstrated point-scanning approaches, which would help application in areas that require high speed processing. Although expanding the limited field of view to a technologically useful size remains an open challenge.

[1]E. Hecht, *Optics*, 4th ed. (Addison-Wesley, 2002).

[2]G. B. Airy, Trans. Cambridge Philoso. Soc. **5**, 283–291 (1835).

[3]G. T. D. Francia, Il Nuovo Cimento **9**, 426 (1952).

[4]J. Lindberg, J. Opt. **14**, 083001 (2012).

[5]Z. S. Hegedus, Opt. Acta: Int. J. Opt. **32**, 815–826 (1985).

[6]Z. S. Hegedus and V. Sarafis, JOSA A **3**, 1892–1896 (1986).

[7]M. Bertero, P. Boccacci, R. E. Davies, F. Malfanti, E. R. Pike, and J. G. Walker, Inverse Prob. **8**, 1 (1992).

[8]M. M. Corral, P. Andres, J. O. Castaneda, and G. Saavedra, Opt. Commun. **119**, 491–498 (1995).

[9]M. M. Corral, P. Andres, C. J. Z. Rodrigues, and C. J. R. Sheppard, Optik **107**, 145–148 (1998).

[10]R. K. Amineh and G. V. Eleftheriades, Opt. Express **21**, 8142–8156 (2013).

[11]A. M. H. Wong and G. V. Eleftheriades, Sci. Rep. **3**, 1715 (2013).

[12]A. Kempf, J. Math. Phys. **41**, 2360 (2000).

[13]M. V. Berry and S. Popescu, J. Phys. A: Math. Gen. **39**, 6965–6977 (2006).

[14]F. M. Huang, N. Zheludev, Y. Chen, and J. F. Garcia de Abajo, Appl. Phys. Lett. **90**, 091119 (2007).

[15]E. T. F. Rogers and N. I. Zheludev, J. Opt. **15**, 094008 (2013).

[16]E. T. F. Rogers, J. Lindberg, T. Roy, S. Savo, J. E. Chad, M. R. Dennis, and N. I. Zheludev, Nature Mater. **11**, 432–435 (2012).

[17]M. Mazilu, J. Baumgartl, S. Kosmeier, and K. Dholakia, Opt. Express **19**, 933–945 (2011).

[18]J. Baumgartl, S. Kosmeier, M. Mazilu, E. T. F. Rogers, N. I. Zheludev, and K. Dholakia, Appl. Phys. Lett. **98**, 181109 (2011).

[19]S. Kosmeier, M. Mazilu, J. Baumgartl, and K. Dholakia, J. Opt. **13**, 105707 (2011).

[20]K. Piché, J. Leach, A. S. Johnson, J. Z. Salvail, M. I. Kolobov, and R. W. Boyd, Opt. Express **20**, 26424–26433 (2012).

[21]E. T. F. Rogers, S. Savo, J. Lindberg, T. Roy, M. R. Dennis, and N. I. Zheludev, Appl. Phys. Lett. **102**, 031108 (2013).

[22]See supplementary material at http://dx.doi.org/10.1063/1.4882246 for more detail on the choice of parameters for Figs. 1 and 2 and additional experimental data showing two more object-image distance pairs.

[23]J. W. Goodman, *Introduction to Fourier Optics*, 3rd ed. (Roberts & Company Publishers, 2005).